

Flow aeration, cavity processes and energy dissipation on flat and pooled stepped spillways for embankments

Philipp Guenther · Stefan Felder · Hubert Chanson

Received: 15 November 2012 / Accepted: 9 March 2013 / Published online: 27 March 2013
© Springer Science+Business Media Dordrecht 2013

Abstract The design floods of several reservoirs were recently re-evaluated and the revised spillway outflow could result in dam overtopping with catastrophic consequences for some embankment structures. Herein a physical study was performed on flat and pooled stepped spillways with a slope typical of embankments ($\theta = 26.6^\circ$) and four stepped configurations were tested: a stepped spillway with flat horizontal steps, a pooled stepped spillway, and two stepped spillways with in-line and staggered configurations of flat and pooled steps. The focus of the study was on the flow aeration, air–water flow properties, cavity flow processes, and energy dissipation performances. The results demonstrated the strong aeration of the flow for all configurations. On the in-line and staggered configurations of flat and pooled steps, the flow was highly three-dimensional. The residual head and energy dissipation rates at the stepped chute downstream end were calculated based upon the detailed air–water flow properties. The results showed that the residual energy was the lowest for the flat stepped weir. The data for the stepped spillway configuration with in-line and staggered configurations of flat and pooled steps showed large differences in terms of residual head in the transverse direction. Altogether the present results showed that, on a 26.6° slope stepped chute, the designs with in-line and staggered configurations of flat and pooled steps did not provide any advantageous performances in terms of energy dissipation and flow aeration, but they were affected by three-dimensional patterns leading to some flow concentration.

Keywords Stepped spillways · Flow aeration · Cavity ejection processes · Energy dissipation · Pooled steps · Residual head · Physical modelling

Philipp Guenther · Stefan Felder · Hubert Chanson (✉)
School of Civil Engineering, The University of Queensland, Brisbane, QLD 4072, Australia
e-mail: h.chanson@uq.edu.au
URL: <http://www.uq.edu.au/~e2hchans/>

1 Introduction

Worldwide the design floods of several reservoirs were re-evaluated and the revised spillway outflow was often larger than the original design one. The occurrence of such large floods could result in dam overtopping with catastrophic consequences for embankment structures when an insufficient storage and spillway capacity is available. During the last decades, a number of overtopping protection systems were developed for embankment structures and earthfill dams. These include concrete overtopping protection systems, timber cribs, sheet-piles, riprap and gabions, reinforced earth, minimum energy loss (MEL) weirs, in-built spillway dams, embankment overflow stepped spillways and the precast concrete block protection systems developed by the Russian engineers [2,9,10,26]. A number of embankment dam stepped spillways were built with a range of design and construction techniques, including gabions, Reno mattresses, reinforced earth, pre-cast concrete slabs and roller compacted concrete (RCC) [5,6]. The stepped profile allows an increased rate of energy dissipation on the spillway chute [6,27] and the design engineers must assess accurately the turbulent kinetic energy dissipation down the staircase chute, in particular for the large discharges per unit width corresponding to the skimming flow regime. A characteristic feature of skimming flows is the high level of turbulence and free-surface aeration [4,29,31]. The water flows down the steps as a coherent free-stream skimming over the pseudo-bottom formed by the step edges, while the turbulent recirculation in the step cavities is maintained through the transmission of shear stress from the free-stream. At the free-surface, air is continuously entrained and released, and the resulting two-phase mixture interacts with the flow turbulence yielding some intricate air–water structures associated with complicated energy dissipation processes [15,24].

In recent years, the air–water flows on pooled stepped spillways were researched in a few studies (Table 1). André [1] and Kökpınar [25] investigated the air entrainment processes on flat, pooled and a combination of flat and pooled steps with channel slopes of 18.6° and 30° . Thorwarth [33] researched the self-induced instabilities on pooled stepped spillways with slopes of 8.9° and 14.6° . Recently Felder et al. [22] conducted a detailed study of the air–water flow properties on a stepped spillway with flat, pooled and combination of flat and pooled steps with a slope of 8.9° . Figure 1a shows a prototype pooled stepped spillway. A related form of pooled stepped chutes is some stepped fishway design. Figure 1b shows a fishway designed with a staggered combination of flat and pooled steps. This particular structure cannot be considered successful however, because some flow concentration yielded some very high velocities at the downstream end of the fish passage which were detrimental to the upstream fish migration.

While the prediction of turbulent dissipation constitutes a critical design stage, the modern literature is skewed towards steep slope designs with flat horizontal steps, typical of modern gravity dams. This paper presents some new physical experiments conducted in a large facility with a channel slope of 26.6° (2H:1V) and step heights of 0.10 m. Such flow conditions would be representative of some stepped storm waterways during flood events and could be considered as a 2:1 to 20:1 scale study of the prototype chutes seen in Fig. 1. Four stepped geometries were tested: flat horizontal steps, pooled steps, and in-line and staggered configurations of flat and pooled steps (Fig. 2). The focus of the present work was on the flow aeration, cavity ejection processes and energy dissipation performances. The results emphasise the complicated nature of turbulent air–water flows on stepped spillways. Herein the aim of the study is a detailed characterisation of the turbulent flow properties supported by detailed air–water flow properties in the skimming flow regime.

(A)



(B)



Fig. 1 Photographs of pooled stepped structures. **a** Pooled stepped spillway of Le Pont dam (France) in June 1998—*Left* looking downstream, *Right* looking upstream. **b** Fishway structure on the Okura River (Japan) on 9 October 2012—The stepped channel consists of a staggered combination of flat and pooled steps

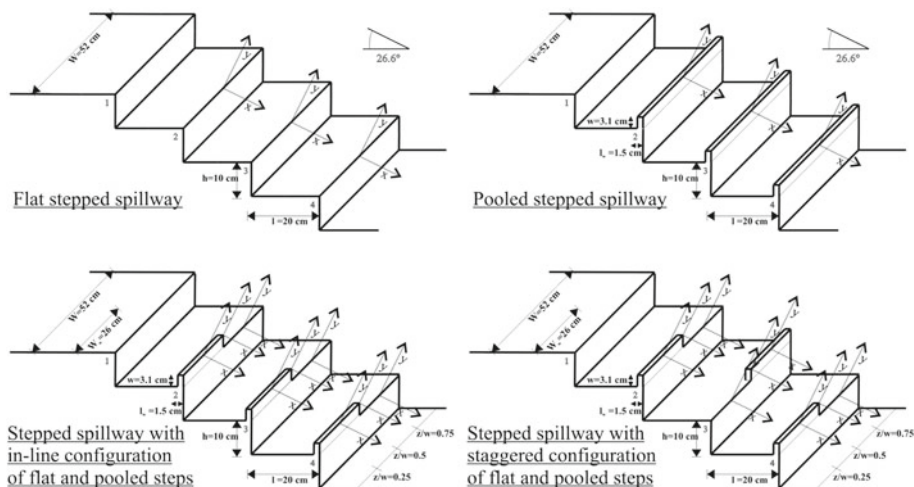


Fig. 2 Definition sketch of the stepped configurations

2 Physical modelling and instrumentation

2.1 Presentation

In a free-surface skimming flow down a stepped spillway, a dimensional analysis gives a series of dimensionless relationships between the two-phase flow properties at a dimensionless location along the chute and the channel characteristics, inflow properties and fluid properties [8, 13, 19]:

$$C, \frac{V}{\sqrt{g \times d_c}}, \frac{u'}{V}, T_{\text{int}} \times \sqrt{\frac{g}{d_c}}, \frac{L_{xz}}{d_c}, \frac{d_{ab}}{d_c}, \frac{F \times d_c}{V_c} = F \left(\frac{x}{d_c}, \frac{y}{d_c}, \frac{z}{d_c}, \frac{w}{h}, \frac{w}{l}, \frac{l_w}{d_c}, \frac{W_w}{W}, \frac{d_c}{h}, \rho_w \times \frac{V \times D_H}{\mu_w}, \frac{g \times \mu_w^4}{\rho_w \times \sigma^3}, \frac{W}{d_c}, \theta, \frac{k_s'}{d_c} \right) \quad (1)$$

where C is the void fraction, V is the interfacial velocity, u' is a turbulent velocity fluctuation, d_c is the critical flow depth, D_H is the hydraulic diameter, q is the water discharge per unit width, W is the channel width, h is the vertical step height, l is the step length, w is the pool weir height for a pooled stepped spillway, l_w is the horizontal pool weir length, W_w is the width of the pooled and flat part in the staggered and in-line configurations of flat and pooled steps, g is the gravity acceleration, θ is the chute slope, u' is the characteristic turbulent velocity, T_{int} is the integral turbulent time scale, L_{xz} is the integral turbulent length scale, x , y , z are respectively the longitudinal, normal and transverse coordinates, μ_w is the dynamic viscosity of water, ρ_w is the water density, σ is the surface tension between air and water, F is the bubble count rate, d_{ab} is the characteristic bubble size and k_s' is the equivalent sand roughness height of the step surface.

Equation (1) expresses the dimensionless air–water flow properties at a location (x, y, z) as functions of the relevant dimensionless parameters, including Froude and Reynolds numbers. In Eq. (1), the dimensionless discharge d_c/h is proportional to a Froude number defined in terms of the step height: $d_c/h = (q^2/\sqrt{g \times h^3})^{1/3}$. Herein the same fluids were used in model and prototype: that is, the Morton number $Mo \propto g \times \mu_w^4/(\rho_w \times \sigma^3)$ was an invariant [11, 30, 36]. Similarly, the chute slope h/l , the channel width W , the horizontal pool weir length l_w and the

Table 1 Summary of experimental studies of air–water flow properties on pooled stepped spillway configurations

Reference (1)	θ (°) (2)	Step geometry (3)	Flow conditions (4)	Instrumentation (5)	Comment (6)
Kökpınar [25]	30	Flat steps: $h = 6$ cm, $l = 10.4$ cm Pooled steps: $h = 6$ cm, $l = 10.4$ cm, $w = 3$ cm Combination of flat/pooled steps: $h = 6$ cm, $l = 10.4$ cm, $w = 3$ cm	$Q = 0.03\text{--}0.100$ m ³ /s, $Re = 2.4 \times 10^5\text{--}8.0 \times 10^5$	Double-tip fiber-optical probe ($\varnothing = 0.08$ mm)	$W = 0.5$ m, 64 steps, $l_w = 2.6$ cm
André [1]	18.6 30	Flat steps: $h = 6$ cm, $l = 17.8$ cm Pooled steps: $h = 6$ cm, $l = 17.8$ cm, $w = 3$ cm Combination of flat/pooled steps: $h = 6$ cm, $l = 17.8$ cm, $w = 3$ cm Flat steps: $h = 6$ cm, $l = 10.4$ cm Pooled steps: $h = 6$ cm, $l = 10.4$ cm, $w = 3$ cm Combination of flat/pooled steps: $h = 6$ cm, $l = 10.4$ cm, $w = 3$ cm	$Q = 0.02\text{--}0.130$ m ³ /s, $Re = 1.6 \times 10^5\text{--}1.0 \times 10^6$	Double-tip fiber-optical probe ($\varnothing = 0.08$ mm)	$W = 0.5$ m, 42/64 steps, $l_w = 2.6$ cm
Thorwarth [33]	8.9 14.6	Pooled steps: $h = 5$ cm, $l = 31.9$ cm, $w = 0\text{--}5$ cm Pooled steps: $h = 5$ cm, $l = 19.2$ cm, $w = 0\text{--}5$ cm	$Q = 0.025\text{--}0.117$ m ³ /s, $Re = 2.0 \times 10^5\text{--}9.3 \times 10^5$	Double-tip conductivity probe ($\varnothing = 0.13$ mm)	$W = 0.5$ m, 22/26 steps, $l_w = 1.5$ cm
Felder et al. [22]	8.9	Flat steps: $h = 5$ cm, $l = 31.9$ cm Pooled steps: $h = w = 5$ cm, $l = 31.9$ cm Combination of flat/pooled steps: $h = w = 5$ cm, $l = 31.9$ cm	$Q = 0.018\text{--}0.117$ m ³ /s, $Re = 1.4 \times 10^5\text{--}9.3 \times 10^5$ $Q = 0.027\text{--}0.117$ m ³ /s, $Re = 2.2 \times 10^5\text{--}9.3 \times 10^5$ $Q = 0.027\text{--}0.117$ m ³ /s, $Re = 2.2 \times 10^5\text{--}9.3 \times 10^5$	Double-tip conductivity probe ($\varnothing = 0.13$ mm)	$W = 0.5$ m, 21 steps, $l_w = 1.5$ cm

step surface skin roughness k_s were kept constant during the experiments. Some experiments were conducted in the centreline, and others at different transverse locations z/d_c . Hence Eq. (1) could be simplified into:

$$C, \frac{V}{\sqrt{g \times d_c}}, \frac{u'}{V}, T_{\text{int}} \times \sqrt{\frac{g}{d_c}}, \frac{L_{xz}}{d_c}, \frac{d_{ab}}{d_c}, \frac{F \times d_c}{V_c} = F' \left(\frac{x}{d_c}, \frac{y}{d_c}, \frac{z}{d_c}, \frac{w}{h}, \frac{w}{l}, \frac{W_w}{W}, \frac{d_c}{h}, Re \right) \quad (2)$$

Table 1 continued

Present study	26.6	Flat steps: $h = 10$ cm, $l = 20$ cm	$Q = 0.030\text{--}0.113$ m^3/s , $Re =$ $2.3 \times 10^5\text{--}$ 8.7×10^5	Double-tip conductivity probe	$W = 0.52$ m,
		Pooled steps: $h =$ 10 cm, $l = 20$ cm, $w = 3.1$ cm	$Q = 0.013\text{--}0.130$ m^3/s , $Re =$ $1.0 \times 10^5\text{--}$ 9.9×10^5	($\varnothing = 0.25$ mm); Array of 2 single- tip conductivity probes	10 steps,
		In-line configura- tion (Pooled and flat steps in-line): $h =$ 10 cm, $l = 20$ cm, $w = 3.1$ cm, $W_w =$ 26 cm	$Q = 0.016\text{--}0.113$ m^3/s , $Re =$ $1.4 \times 10^5\text{--}$ 8.7×10^5	($\varnothing = 0.35$ mm)	$l_w = 1.5$ cm
		Staggered configura- tion (Pooled and flat staggered): $h =$ 10 cm, $l = 20$ cm, $w = 3.1$ cm, $W_w =$ 26 cm	$Q = 0.030\text{--}0.113$ m^3/s , $Re =$ $2.3 \times 10^5\text{--}$ 8.7×10^5		

Notes θ channel slope, h step height, l step length, w weir height, l_w pool weir length, W channel width, Q water discharge, Re Reynolds number defined in terms of hydraulic diameter, W_w width of pooled stepped sections in in-lined and staggered configurations

where Re is the Reynolds number: $Re = \rho_w \times V \times D_H / \mu_w$. The physical experiments are traditionally conducted based upon an undistorted Froude similitude, although it is nearly impossible to achieve a true dynamic similarity of high-velocity air–water flows in small size laboratory models because of the number of relevant dimensionless parameters ([8], pp. 358–263, [11]). Recent results demonstrated that the physical studies must be conducted in large size facilities operating at large Reynolds numbers to minimise viscous scale effects [19]. Herein the study was performed based upon an undistorted Froude similarity and the experimental flow conditions (Table 1) were selected to achieve large dimensionless discharges corresponding to Reynolds numbers ranging from 1×10^5 to 1×10^6 .

2.2 Physical facility and instrumentation

New experiments were performed at the University of Queensland on a large size stepped spillway model with a slope of 26.6° . The experimental facility was newly designed. The stepped spillway consisted of 10 steps with step height $h = 10$ cm, and step length of $l = 20$ cm. The chute had a width $W = 0.52$ m. The steps were made out of plywood and the channel walls out of perspex. Constant flow rates were supplied by a large upstream intake basin with a size of $2.9 \text{ m} \times 2.2 \text{ m}$ and a depth of 1.5 m. A smooth inflow was supplied by a 1.01 m long smooth sidewall convergent with a $4.23:1$ contraction ratio. At the upstream end of the test section, the flow was controlled by a broad-crested weir with height of 1 m, width $W = 0.52$ m, length $L_{\text{crest}} = 1.01$ m and an upstream rounded corner ($r = 0.08$ m). The broad-crested weir was previously tested and some detailed velocity and pressure measurements [20] provided the discharge calibration curve used in the present study:

$$\frac{Q}{W} = \left(0.92 + 0.153 \times \frac{H_1}{L_{\text{crest}}} \right) \times \sqrt{g \times \left(\frac{2}{3} \times H_1 \right)^3} \quad 0.02 \leq H_1/L_{\text{crest}} \leq 0.3 \quad (3)$$



Fig. 3 Photographs of the stepped configurations including in-line and staggered stepped arrangements (Bottom) View from upstream looking downstream (a, Left) Flat stepped arrangement (b, Right) Pooled stepped arrangement (c, Left) In-line stepped arrangement (d, Right) Staggered stepped arrangement

where Q is the water discharge and H_1 is the upstream total head measured using a point gauge.

At the downstream end, the stepped chute was followed by a smooth horizontal raceway ending with an overfall into the recirculation sump pit. The flow was supercritical in the horizontal raceway and did not interfere with the stepped chute flow.

The air–water flow measurements were conducted with either a two-tip phase-detection intrusive probe ($\varnothing = 0.25\text{mm}$, $\Delta x = 7.2\text{mm}$, $\Delta z = 1.5\text{mm}$) or an array of two single-tip phase-detection probes ($\varnothing = 0.35\text{mm}$) separated by a range of well-defined transverse distances $3.5 < \Delta z < 81\text{mm}$. Herein Δx is the longitudinal distance between probe sensors and Δz is the transverse distance between sensors. The probe sensors were excited by an air bubble detector (Ref. UQ82.518) and sampled at 20 kHz per tip for 45 s. All conductivity probe tips were mounted on a trolley and their elevation in the direction perpendicular to the pseudo-bottom formed by the step edges (i.e. y -direction) was controlled by a fine adjustment screw-drive mechanism equipped with a MitutoyoTM digital ruler (accuracy $< 0.1\text{ mm}$).

Further observations were conducted with a HD video camera SonyTM HDR-XR160E (Standard HQ HD quality 25 fps), two dSLR camera PentaxTM K-7 and CanonTM 450D. More details on the experimental facility, instrumentation and experimental data were reported in [23].

2.3 Signal processing

The raw data recorded with the double-tip conductivity probe yielded the void fraction C , the bubble count rate F , the interfacial velocity V , and the turbulence intensity Tu . For all



Fig. 4 Skimming flow regime on flat and pooled stepped spillways. **a** Flat steps, $Q = 0.114 \text{ m}^3/\text{s}$, $d_c/h = 1.7$, $Re = 8.8 \times 10^5$. **b** Pooled steps, $Q = 0.100 \text{ m}^3/\text{s}$, $d_c/h = 1.56$, $Re = 7.7 \times 10^5$

experiments, the void fraction, bubble frequency and particle chord sizes were calculated based upon a single-threshold technique with a threshold set at 50 % of the air–water range [34]. The interfacial velocity, turbulence intensity and integral turbulent scales were calculated using some correlation technique [7, 12].

The data for the array of the two single-tip probes provided the transverse integral turbulent time and length scales T_{int} and L_{xz} . An integration of the maximum cross-correlation values $(R_{\text{xz}})_{\text{max}}$ between the raw data of the two single-tip probes with various spacing Δz gave the integral turbulent length scale [12]:

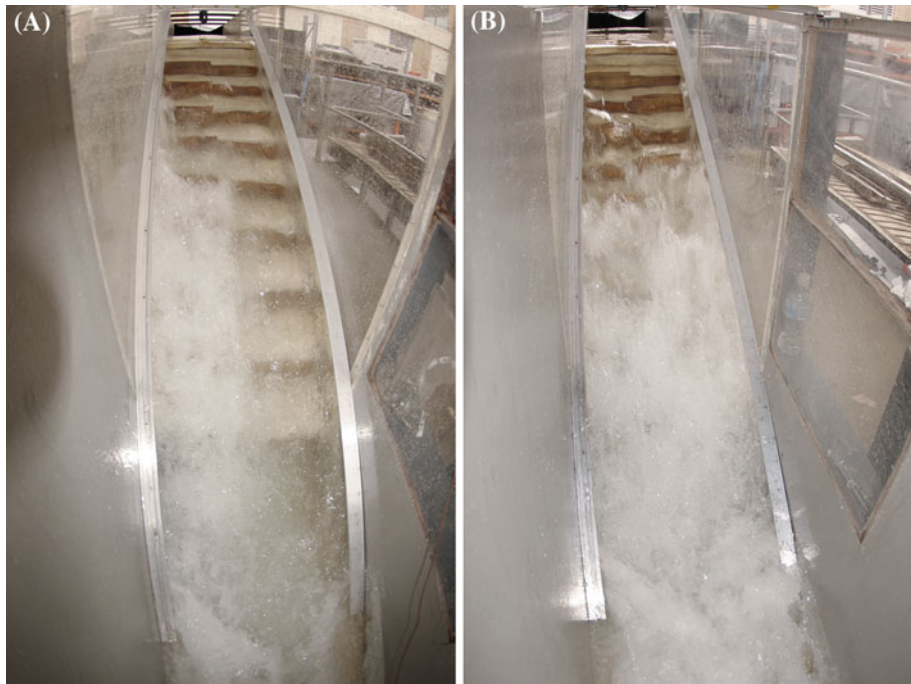


Fig. 5 Three-dimensional skimming flows down the in-line and staggered configurations of flat and pooled steps (**a**, *Left*) In-line configuration, $Q = 0.098 \text{ m}^3/\text{s}$, $d_c/h = 1.54$, $Re = 7.6 \times 10^5$ (**b**, *Right*) Staggered configuration, $Q = 0.090 \text{ m}^3/\text{s}$, $d_c/h = 1.45$, $Re = 6.9 \times 10^5$

$$L_{xz} = \int_{z=0}^{z=z((R_{xz})_{\max}=0)} (R_{xz})_{\max} \times dz \quad (4)$$

The corresponding integral turbulent time scale was also calculated:

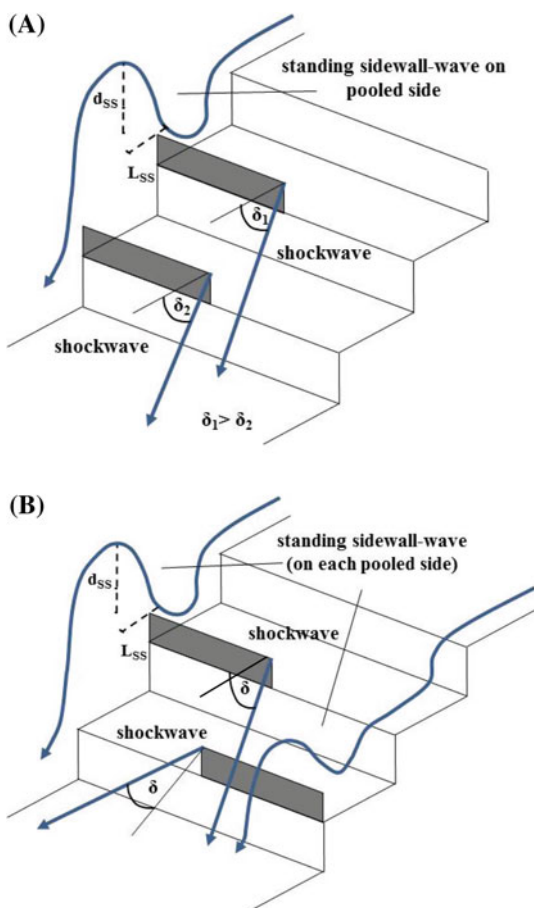
$$T_{\text{int}} = \frac{1}{L_{xz}} \times \int_{z=0}^{z=z((R_{xz})_{\max}=0)} (R_{xz})_{\max} \times T_{xz} \times dz \quad (5)$$

where T_{xz} is the cross-correlation integral time scale calculated in an integration from the maximum of the cross-correlation function until the first crossing.

2.4 Experimental investigations

The experimental study was conducted for four stepped spillway configurations (Figs. 2, 3). These were a stepped spillway with flat horizontal steps, a pooled stepped spillway with weir height $w = 0.031 \text{ m}$, and two stepped spillways with in-line and staggered configurations of flat and pooled steps ($w = 0.031 \text{ m}$). The in-line stepped spillway configuration consisted of pooled and flat steps in-line for half the channel width ($W_w = W/2 = 0.26 \text{ m}$). The staggered pooled stepped spillway configuration was characterised by alternating flat and pooled steps. On the flat and pooled stepped spillways, the air–water flow measurements were conducted

Fig. 6 Definition sketches of sidewall standing waves and shock waves in stepped chutes with in-line and staggered configurations of flat and pooled steps. **a** In-line configuration of flat and pooled steps. **b** Staggered configuration of flat and pooled steps



on the channel centreline. For the in-line and staggered configurations, the measurements were performed at three transverse locations: $z/W = 0.25, 0.5$ (centreline) and 0.75 .

The flow patterns were observed for a wide range of discharges: $0.002 \leq Q \leq 0.155 \text{ m}^3/\text{s}$. The air–water flow measurements were performed for discharges within $0.013 \leq Q \leq 0.130 \text{ m}^3/\text{s}$ corresponding to Reynolds numbers between 1×10^5 and 1×10^6 . Most two-phase flow experiments were conducted in the transition and skimming flow regimes (see below).

3 Flow patterns

The visual observations of flow patterns were conducted for all stepped spillway configurations for a broad range of discharges. For some low discharges, the air–water flows on the pooled stepped spillway exhibited some small instabilities linked with some flow pulsations. The flow processes on the stepped spillways with in-line and staggered configurations of flat and pooled steps showed some strongly three-dimensional air–water flow features including standing sidewall waves and supercritical shockwaves.

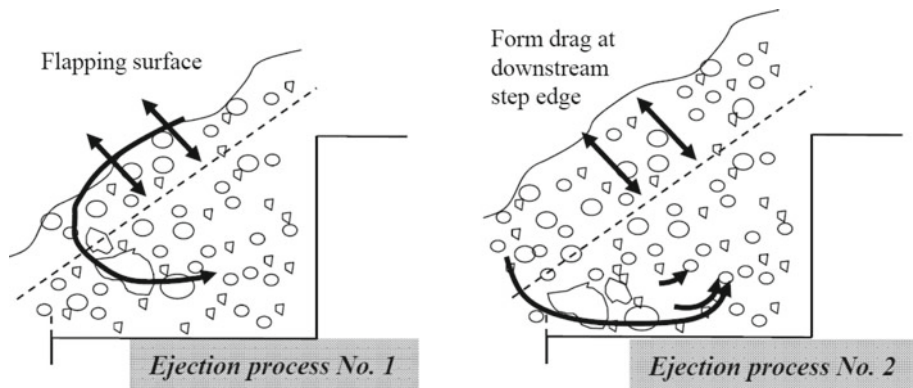


Fig. 7 Sketch of cavity ejection processes on flat and pooled stepped spillways ($\theta = 26.6^\circ$)

The flat stepped spillway showed some typical flow patterns with nappe ($d_c/h < 0.5$), transition ($0.5 < d_c/h < 0.9$) and skimming flow ($d_c/h > 0.9$) regimes depending upon the dimensionless flow rate d_c/h . The findings were comparable to a number of earlier studies [5,6,18,27]. Some similar flow regimes were observed on the pooled stepped spillway (Fig. 4), although some pulsating flow was seen for a range of nappe flow rates. For the smallest flow rates ($d_c/h < 0.45$), a nappe flow regime was seen and the water discharged in a succession of free-falling nappes from one step pool to the following one. However, for $0.3 \leq d_c/h \leq 0.45$, a pulsating flow was observed in the first pooled step cavity leading to some small instability of the following free-falling nappes. The pulsations in the first pooled step cavity were periodic and had a frequency of about 1 Hz (1 s period) for $d_c/h = 0.3$. These pulsations were seen about every 5 s for $d_c/h = 0.45$. The pulsating mechanism was comparable to the self-induced instabilities on pooled stepped spillways with slopes $\theta = 8.9^\circ$ and 30° [21,32,33]. For intermediate flow rates $0.45 \leq d_c/h \leq 0.97$, a transition flow regime was observed associated with some strong splashing in the air–water flow region downstream of the inception point of free-surface aeration. For larger discharges $d_c/h > 0.97$, a skimming flow regime took place with some stable recirculation motion in the pooled step cavities (Fig. 4b). At the upstream end of the chute, the flow was transparent (clear-waters) and the water surface was parallel to the pseudo-bottom formed by the pool step weirs equivalent to skimming flows on flat stepped spillways. The flow depth however was larger than on flat stepped chutes because of the pool height. Downstream of the inception point of free-surface aeration, the flow was highly aerated.

On the in-line and staggered configurations of flat and pooled steps, the flow was highly three-dimensional (Figs. 5, 6). This is illustrated in Figs. 5 and 6 presenting some schematics of the three-dimensional flow motion. Standing sidewall waves and shockwaves were observed along the sidewalls and on channel centreline respectively (Fig. 6), and these instabilities were associated with some strong splashing. On the in-line stepped configuration, the pool weirs induced larger air–water depths at the pooled side of the channel, and a faster flow motion was observed at the flat stepped side (Fig. 5a). The formation of nappe, transition and skimming flows could be determined separately on both sides. For small flow rates ($d_c/h < 0.46$), a nappe flow regime was observed on both sides of the spillway chute with plunging jets from step to step on the flat side and from pool to pool on the pooled side. Some transverse flow motions as well as strong droplet ejections were seen along the entire channel

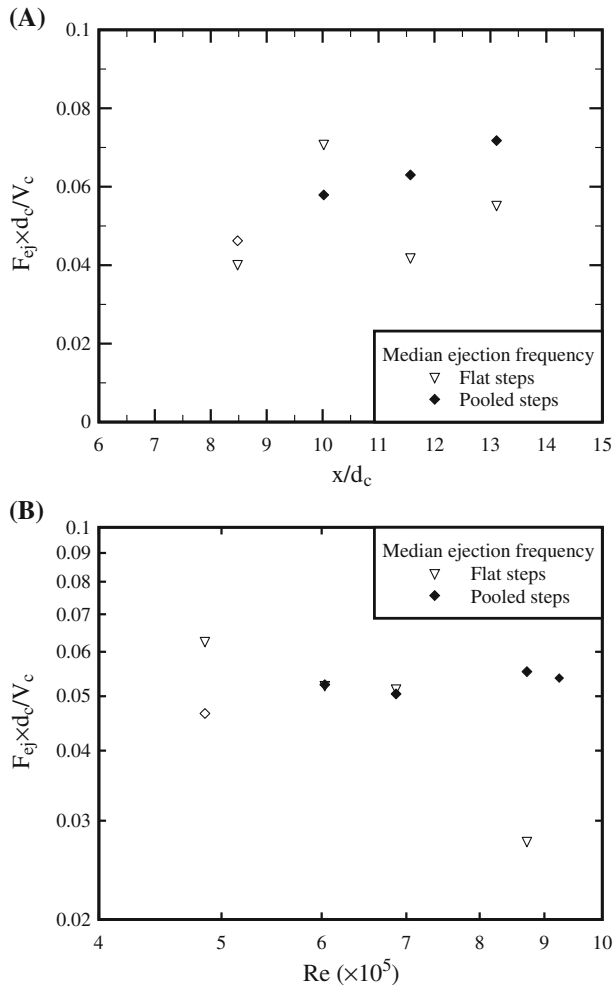


Fig. 8 Dimensionless cavity ejection frequency $F_{ej} \times d_c / V_c$ on flat and pooled stepped spillways ($\theta = 26.6^\circ$). **a** Longitudinal distribution in skimming flow ($d_c/h = 1.45$, $Re = 6.9 \times 10^5$). **b** Median ejection frequency as a function of the Reynolds number

length. With increasing discharges ($0.46 < d_c/h < 0.57$), the flow became more unstable: it was characterised by plunging jets interacting on channel centreline together with a chaotic flow behaviour. The pools induced large flow disturbances and some three-dimensional flow motion was observed. For $0.57 < d_c/h < 0.86$, a transition flow regime was observed on both sides of the channel with some distinct droplet ejection downstream of the inception point of aeration. Some transverse flow interactions took place on channel centreline and yielded some three-dimensional flow motions along the entire channel. An intermediate flow regime ($0.86 < d_c/h < 1.03$) was characterised by a skimming flow regime on the pooled stepped side, and some transition flow on the flat stepped side of the spillway. Overall the three-dimensional flow motion and flow disturbances caused by the pools became less significant with increasing discharges. For $d_c/h > 1.03$, a skimming flow was observed on both

sides of the channel. The skimming flows showed some similarities to those observed on the flat stepped and pooled stepped spillways (Fig. 5a). The flow showed comparatively larger droplet ejections and the recirculation processes in the cavities appeared more irregular and disturbed compared to the uniform flat and pooled stepped spillways.

On the staggered stepped configuration, a nappe flow regime was observed at low flow rates ($d_c/h < 0.56$). A wavy flow appearance from side to side was observed along the entire channel length. The jets were highly aerated and showed some distinct plunge heights. For $0.56 < d_c/h < 0.92$, a transition flow occurred along the stepped chute. Some jets plunged over each second adjacent step edge. The step cavities of both flat and pooled steps showed no air pockets. The air–water mixture was highly aerated, showing some pseudo-chaotic pattern and transverse interactions on the channel centreline. The waving appearance of the flow from side to side became less significant than in the nappe flow regime. For $d_c/h > 0.92$, a skimming flow regime was observed (Fig. 5b). The recirculation in the step cavities was observed, although the recirculation processes were unsteady and disturbed by the staggered stepped configuration. The flow appeared highly aerated.

The stepped spillways with in-line and staggered configuration of flat and pooled steps showed some irregular occurrence of standing sidewalls and shockwaves for all flow regimes. The side-wall standing wave lengths and heights were comparable for both in-line and staggered configurations of flat and pooled steps. With increasing discharges, both wave height and length became smaller. The shockwaves occurred predominantly on the spillway centreline and the direction of the shockwaves differed between adjacent steps depending upon the configuration (Fig. 6). Further informations on and photographs of the flow instabilities were reported by [23].

4 Cavity flow processes

On the flat and pooled stepped spillways, the cavity ejection processes were investigated using video-cameras and high-shutter speed photography. The recirculation processes were documented for each step cavity at and downstream of the inception point of free-surface aeration. The clear-water surface upstream of the inception point appeared two-dimensional and parallel to the pseudo-bottom formed by the step edges and pooled weir edges respectively. Close to the inception point, the surface showed an irregular flapping mechanism which led to some waving behaviour. The surface tended to lean inward the cavity at irregular intervals and caused an air packet entrapment which was advected in the form of smaller and uniform shaped bubbles within the step cavities (Fig. 7, Left). This pattern was consistent with previous observations on stepped spillways [3, 6, 35]. With increasing discharge, the flapping mechanism of the free-surface became less distinct. Visually the flow resistance caused by the next downstream step, or pool edge, yielded some ejection processes close to the respective step or pool edge. Figure 7 illustrates the flapping mechanism and the cavity ejection processes on the flat and pooled stepped spillways. The cavity ejection processes were similar in appearance for the flat and pooled steps.

Basically the cavity flow observations highlighted some distinct ejection processes with inward and outward cavity flow motion. These occurred at irregular time intervals and were associated with some additional air entrainment. The ejections appeared to be sequential from upstream to downstream as illustrated by Djenidi et al. [17] and Chanson et al. [16]. On average, the flat stepped data indicated a nearly constant cavity ejection rate independently of downstream distance for a given flow rate (Fig. 8a), although the pooled steps data indicated a monotonic increase with increasing distance for $8 < x/d_c < 13$. The overall results are

summarised in Fig. 8b showing the median cavity ejection frequency as a function of the Reynolds number. Indeed the ejection processes took place in regions of high shear stress where the Reynolds number was closely linked to turbulence properties.

The cavity ejection process in a skimming flow on stepped spillway may be analysed in term of energy considerations, assuming that all the energy losses took place by viscous dissipation in the cavity, with some energy exchange between the mainstream and the recirculation by irregular fluid ejection (Chanson and Toombes 2011, [16]). The results yielded an expression of the averaged ejection frequency F_{ej} as a function of the Darcy–Weisbach friction factor for air–water flow f_e :

$$\frac{F_{ej} \times (h \times \cos \theta)}{U_w} \approx \frac{f_e}{2 \times \lambda \times \eta} \quad (6)$$

where U_w is the main flow velocity, λ is the ratio of average fluid ejection volume to total cavity volume, and η is the ratio of average ejection period to burst duration. Equation (6) was developed for a wide chute with flat horizontal steps assuming a gradually-varied flow motion close to uniform equilibrium [16]. The reasoning may be extended to a pooled stepped chute:

$$\frac{F_{ej} \times (h \times \cos \theta)}{U_w} \approx \frac{f_e}{2 \times \lambda \times \eta \times (1 + 2 \times \frac{w}{h})} \quad (7)$$

Equation (7) is valid for a wide chute with horizontal steps and vertical pool walls.

Herein the observations indicated that the average ejection period to burst duration was on average $\eta \approx 3.5$. Although the video analyses did not provide accurate information about the average fluid ejection volume ratio, the combination of flow resistance data and Eqs. (6) and (7) would yield meaningless values of λ (i.e. $\lambda > 1$). The finding might suggest the over-simplification of Eqs. (6) and (7) to assume that all the energy losses took place by viscous dissipation in the cavity.

5 Air–water turbulent flow properties

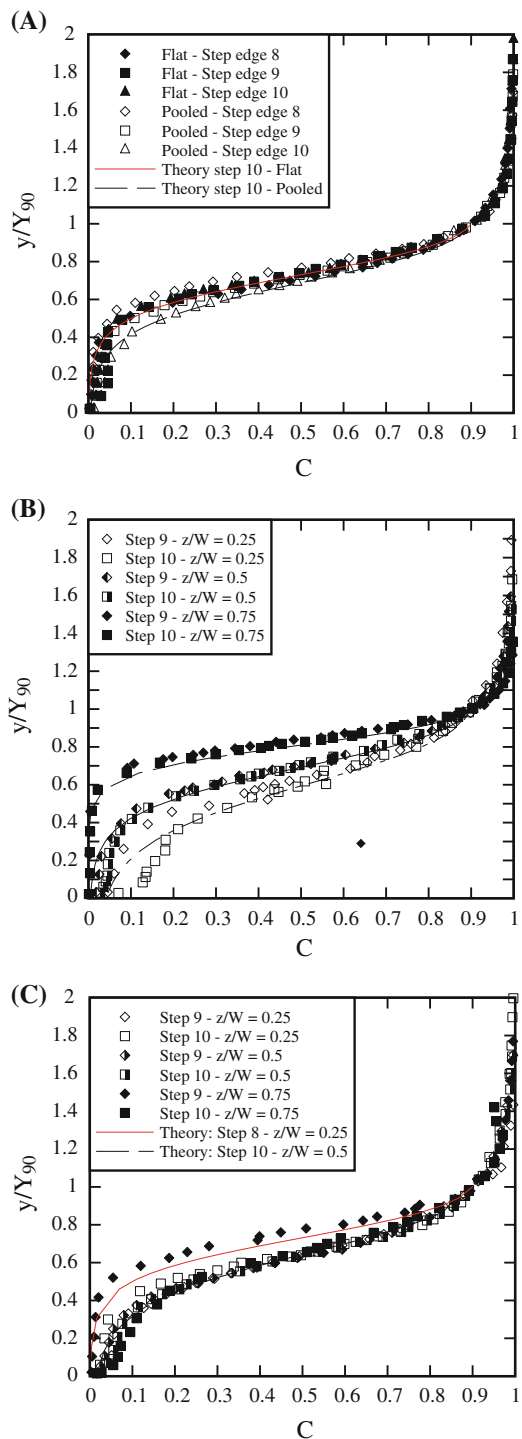
Some detailed air–water flow measurements were performed for all four configurations at all step edges downstream of the inception point of air entrainment. All the data highlighted the intense flow aeration. The entire water column was aerated, including the step cavities. Figure 9 present some typical dimensionless distributions of void fraction for all four stepped configurations. In Fig. 9, y is the distance normal to the pseudo-bottom formed by the step edges with $y = 0$ at the step edges for flat steps and $y = 0$ at the weir edge for the pooled steps. Overall the skimming flow data compared favourably with an analytical solution of the air bubble diffusion equation:

$$C = 1 - \tanh^2 \left(K' - \frac{y/Y_{90}}{2 \times D_o} + \frac{(y/Y_{90} - 1/3)^3}{3 \times D_o} \right) \quad (8)$$

where Y_{90} is the characteristic distance where $C = 0.90$, and K' , D_o are dimensionless functions of the depth-averaged void fraction C_{mean} defined in terms of Y_{90} [15]. Equation (8) is compared with some experimental data in Fig. 9.

Figure 10 shows some typical dimensionless distributions of the bubble count rate $F \times d_c/V_c$ in skimming flows as functions $(y+w)/d_c$. Herein V_c is the critical flow velocity: $V_c = \sqrt{g \times d_c}$. The distribution of bubble count rates showed typical shapes with maxima in

Fig. 9 Dimensionless distributions of void fractions in skimming flows. **a** Flat and pooled steps, $Q = 0.097 \text{ m}^3/\text{s}$, $d_c/h = 1.52$, $\text{Re} = 7.4 \times 10^5$. **b** In-line configuration, $Q = 0.090 \text{ m}^3/\text{s}$, $d_c/h = 1.45$, $\text{Re} = 6.9 \times 10^5$. **c** Staggered configuration, $Q = 0.113 \text{ m}^3/\text{s}$, $d_c/h = 1.70$, $\text{Re} = 8.7 \times 10^5$



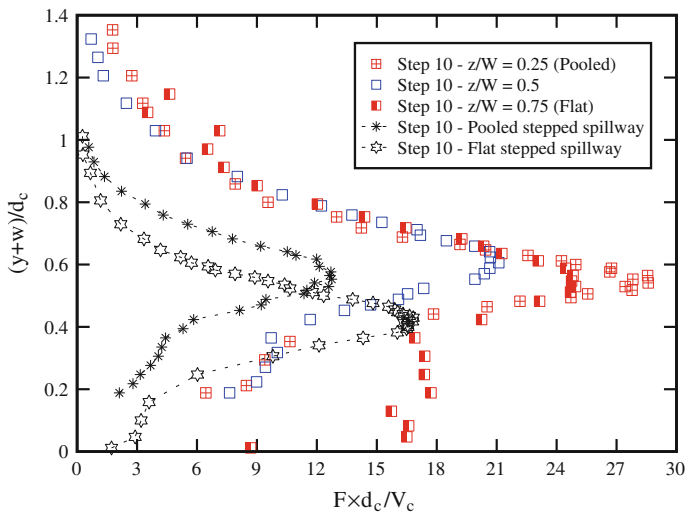


Fig. 10 Dimensionless bubble count rate distributions on the stepped spillway with staggered configuration of flat and pooled steps in skimming flows ($\theta = 26.6^\circ$): $d_c/h = 1.70$, $Q = 0.113 \text{ m}^3/\text{s}$, $Re = 8.72 \times 10^5$ - Comparison with flat and pooled stepped spillways for identical flow conditions

the intermediate flow region for void fractions of about $C = 0.4$ to 0.5 for all configurations. Further the maximum bubble count rate increased with increasing downstream distance from the inception point. Figure 10 includes some staggered stepped data highlighting some transverse differences. The transverse differences were even more pronounced on the in-line stepped configuration with significantly large bubble count rates in on the flat stepped side (data not shown). Overall the staggered configuration data presented the largest bubble count rates, implying a greater potential for air–water mass transfer on that geometry.

The void fraction data showed close results between flat and pooled steps within the main flow (Fig. 9a). In the skimming flow, the depth-averaged void fraction ranged typically between 0.30 and 0.40 for both stepped geometries. On the in-line configuration of flat and pooled steps, the measurements showed some quantitative differences in the transverse direction at each step edge (Fig. 9b). The flow was significantly more aerated on the pooled side ($z/W = 0.25$) as illustrated by the photographs (Fig. 5a). On the staggered configuration of flat and pooled steps, the void fraction distributions were more uniformly distributed across the channel, although the alternation of flat and pooled steps every second step edge induced locally some three-dimensional flow motion and transverse fluxes (Fig. 9c).

The interfacial velocity distributions (data not shown) exhibited a self-similar profile on both flat and pooled stepped spillways comparable to previous studies:

$$\frac{V}{V_{90}} = \left(\frac{y}{Y_{90}} \right)^{1/N} \quad y/Y_{90} < 1 \quad (9a)$$

$$\frac{V}{V_{90}} = 1 \quad y/Y_{90} > 1 \quad (9b)$$

with V_{90} is the characteristic velocity at $y = Y_{90}$. The exact value of N varied slightly from a step edge to the next one for a given flow rate, with a typical value $N = 10$ for all stepped configurations. For comparison, [25] reported $N = 6$ on flat and pooled stepped chutes ($\theta = 30^\circ$). On the in-line and staggered configurations of flat and pooled steps, the velocity distributions followed Eq. (9a) for $y/Y_{90} < 1$ at most transverse locations, but the

velocity data in the spray region (i.e. $y/Y_{90} > 1$) were scattered. On the in-line configuration, the interfacial velocities were consistently larger on the flat stepped side than on the pooled stepped side of the chute. Some transverse flow motion was observed along the channel centreline with the staggered configuration of flat and pooled steps, leading to an alternation of transverse flow direction between each step.

Some typical turbulence intensity distributions are illustrated in Fig. 11a for flat and pooled stepped spillways. All skimming flow data showed relatively large turbulence levels on the stepped chutes and little difference was visible qualitatively and quantitatively between flat and pooled stepped spillways (Fig. 11a). For a given profile, the data showed a local maximum in turbulence intensity in the intermediate flow region ($0.3 < C < 0.7$) between the bubbly flow region and the spray region above. Some measurements of the integral turbulent length scale L_{xz} and the integral turbulent time scale T_{int} were conducted on the flat and pooled stepped spillways. Figure 11b, c present some typical results. The comparative results highlighted the larger integral turbulent lengths scales on the flat stepped chute suggesting larger transverse air–water vortices, while the dimensionless turbulent time scales $T_{int} \times \sqrt{g/d_c}$ were almost identical for the flat and pooled stepped spillways (Fig. 11c). The integral turbulent time and length scale data highlighted some maxima in the intermediate flow region ($0.3 < C < 0.7$) (Fig. 11). All distributions showed very small integral turbulent scale values in the bubbly flow region, while the values of L_{xz} decreased also in the upper spray region (Fig. 11b). On the other hand, some large integral turbulent time scale values were recorded in the upper spray region ($C > 0.97$) for the flat stepped spillway, while the values of T_{int} were smaller on the pooled stepped spillway (Fig. 11c). The reason for the difference remains unknown. The finding might indicate a different nature of ejected droplets above the pooled stepped spillway, although the visual observations did not show any obvious difference in terms of droplet ejections and air–water free-surfaces for both configurations.

6 Energy dissipation

The rate of energy dissipation on the stepped spillway and the residual energy at the downstream end of the stepped chute are some key design parameters. Herein the rate of energy dissipation and the residual energy were estimated for all stepped spillway configurations based upon the detailed air–water flow measurements. The residual head was calculated as:

$$H_{res} = d \times \cos \theta + \frac{U_w^2}{2 \times g} + w = \int_0^{Y_{90}} (1 - C) \times \cos \theta \times dy + \frac{q^2}{2 \times g \times \left(\int_0^{Y_{90}} (1 - C) \times dy \right)^2} + w \quad (10)$$

where d is the equivalent clear-water depth. (Note that the velocity head correction coefficient was about 1.02–1.03, and it would be pointless to include any velocity correction coefficient). On the in-line and staggered configurations of flat and pooled steps, the residual head data were transverse averaged [23]. For the 10-step chute, the rate of energy dissipation ranged from 45 to 90 %, with decreasing rate of energy dissipation with increasing flow rate as previously observed by Chanson [4] and Peruginelli and Pagliara [28]. For the design engineers, the dimensionless residual head H_{res}/d_c is a more relevant design parameter. Present

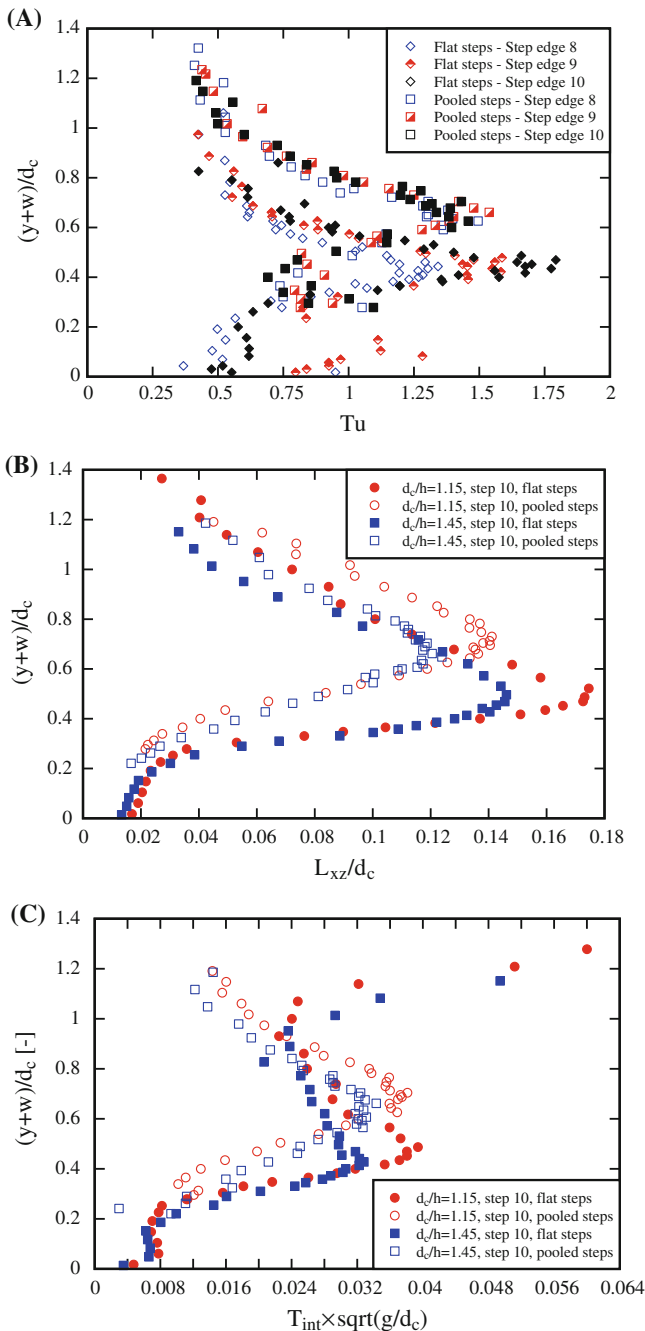


Fig. 11 Dimensionless distributions of turbulence intensity, and integral turbulent length and times scales on flat and pooled stepped spillways. **a** Turbulence intensity Tu —Flow conditions: $d_c/h = 1.15$, $Q = 0.063 \text{ m}^3/\text{s}$, $Re = 4.9 \times 10^5$. **b** Integral turbulent length scale L_{xz}/d_c — Flow conditions: $d_c/h = 1.15$, $Q = 0.063 \text{ m}^3/\text{s}$, $Re = 4.9 \times 10^5$ and $d_c/h = 1.45$, $Q = 0.090 \text{ m}^3/\text{s}$, $Re = 6.9 \times 10^5$. **c** Integral turbulent time scale $T_{int} \times \sqrt{g/d_c}$ —Flow conditions: $d_c/h = 1.15$, $Q = 0.063 \text{ m}^3/\text{s}$, $Re = 4.9 \times 10^5$ and $d_c/h = 1.45$, $Q = 0.090 \text{ m}^3/\text{s}$, $Re = 6.9 \times 10^5$

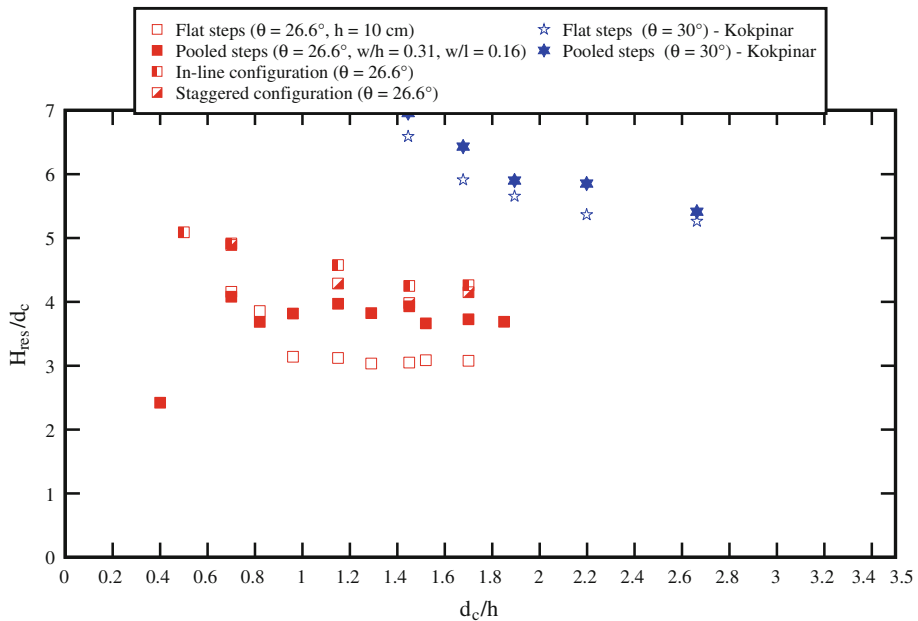


Fig. 12 Dimensionless residual head at the downstream end of the 10-step stepped spillways—Comparison between flat stepped chute, pooled step chute, and in-line and staggered configurations of flat and pooled steps (Present study), as well as with the re-analysed data of [25]—All data were estimated based upon detailed air–water flow measurements

results implied that the dimensionless residual head was about $2.5 \leq H_{\text{res}}/d_c \leq 5$ (Fig. 12). In Fig. 12, the dimensionless residual head is shown as a function of the dimensionless discharge d_c/h . The present data showed the smallest residual head for the flat stepped spillway: i.e., $H_{\text{res}}/d_c \approx 3.1$ on average in skimming flow. The residual head was larger on the pooled stepped spillway: i.e., $H_{\text{res}}/d_c \approx 3.8$ on average, but for the lowest data ($H_{\text{res}}/d_c = 2.3$ for $d_c/h = 0.4$) obtained in nappe flow regime. For the stepped spillways with in-line and staggered configurations of flat and pooled steps, larger residual head data were obtained, with some data scatter.

The data for the in-line and staggered configurations of flat and pooled steps must be considered with care. The results shown in Fig. 12 were transverse averaged. A transverse averaging approach was used to quantify an average air–water flow parameters and energy dissipation across the channel width. The effects of the weighting factors were tested with a sensitivity analysis [23]. Locally the residual head could be significantly larger because of the three-dimensional flow motion. For example, on the in-line geometry, the dimensionless residual head H_{res}/d_c ranged from less than 2 to up to 17 locally, depending upon the transverse location and flow rate, while H_{res}/d_c varied within a factor 2 across the last step for a given flow rate on the staggered geometry.

Overall the present data ($\theta = 26.6^\circ$) showed a larger rate of energy dissipation on the spillway with flat horizontal steps compared to all the other configurations in the skimming flow regime. The result was consistent with the re-analysis of physical data down a 30° stepped chute [25], despite some quantitative difference in residual head levels with the present data (Fig. 9). On a 30° slope, Takahashi et al. [32] observed a comparatively smaller rate of energy dissipation on the flat stepped chute than on the pooled steps for a range of

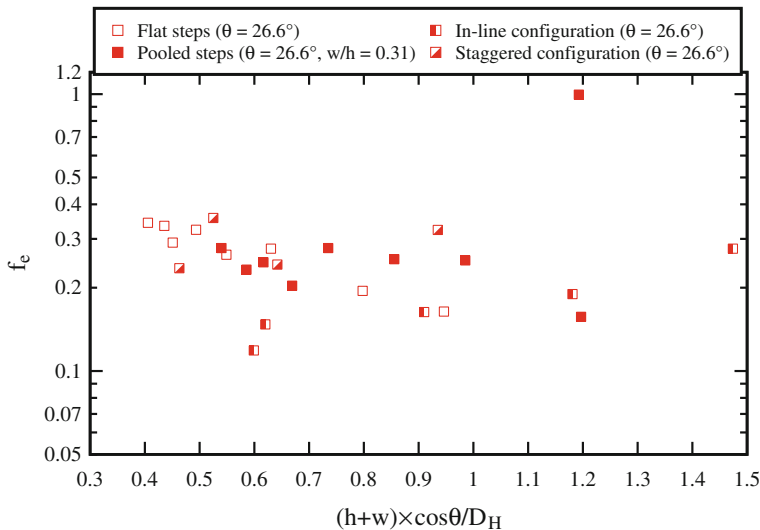


Fig. 13 Darcy friction factors on flat and pooled stepped spillways (all four configurations) - All data were calculated based upon detailed air–water flow measurements

relative pool heights ($0.25 < w/h < 1$), but the study of Takahashi et al. did not rely upon air–water flow measurements. Herein the designs with in-line and staggered configurations of flat and pooled steps did not provide any advantageous performances in terms of energy dissipation, while they were affected by flow instabilities and three-dimensional patterns leading to some flow concentration.

On a stepped spillway, the flow resistance is commonly expressed in the form of a Darcy–Weisbach friction factor f_e [6,31]. The friction factor on a stepped spillway is an average dimensionless shear stress between the air–water main stream and the step cavities. Herein the Darcy–Weisbach friction factor was calculated as:

$$f_e = \frac{8 \times g \times S_f \times \int_0^{Y_{90}} (1 - C) \times dy}{U_w^2} \quad (11)$$

where the friction slope equals $S_f = -\partial H / \partial x$, H is the total head [6,16]. Equation (11) was used to calculate the equivalent Darcy–Weisbach friction factors for the flat and pooled stepped spillway configurations. For the in-line and staggered configurations of flat and pooled stepped steps, the friction factor was based upon a transverse averaging of the air–water flow properties [23]. The friction factor results are illustrated in Fig. 13 as a function of the dimensionless step cavity roughness height $(h+w) \times \cos \theta / D_H$, where D_H is the hydraulic diameter. For the stepped spillways with in-line and staggered configuration of flat and pooled steps, the step roughness cavity height was averaged in the transverse direction. All present data showed some scatter within typically $0.15 < f_e < 0.28$ for the skimming flows (Fig. 13). There was no clear trend in terms of flow resistance. Larger friction factors were observed for the smallest flow rates for all stepped spillway configurations: i.e., $f_e \approx 0.3$ (small flow rates). It is noteworthy that, in the present study ($\theta = 26.6^\circ$), the pooled weir did not increase the flow resistance.

7 Conclusion

A physical study was performed on flat and pooled stepped spillways with a slope typical of embankment spillway ($\theta = 26.6^\circ$ or 1V:2H). Four stepped configurations were systematically tested: (a) a stepped spillway with flat horizontal steps, (b) a pooled stepped spillway with relative weir height $w/l = 0.155$, and two stepped spillways with (c) in-line and (d) staggered configurations of flat and pooled steps. While different stepped chute configurations were tested, the focus of the study was on the flow aeration, air–water flow properties, cavity flow processes, and energy dissipation performances.

The flat stepped spillway showed some typical flow patterns with nappe, transition and skimming flow regimes depending upon the flow rate. Some similar flow regimes were observed on the pooled stepped spillway, although some pulsating flow was seen for some nappe flow rates associated with the downstream propagation of small instabilities. On the in-line and staggered configurations of flat and pooled steps, the flow was highly three-dimensional. Standing sidewall waves and shockwaves were observed along the sidewalls and on channel centreline respectively. These instabilities were instationary and associated with some strong splashing. Detailed air–water flow measurements were conducted downstream of the inception point of free-surface aeration for all configurations. The results highlighted the strong flow aeration for all configurations and all investigated flow conditions. The air–water flow properties highlighted quantitatively the three-dimensional nature of the flow with transverse motion and associated secondary currents, in the in-line and staggered configurations of flat and pooled steps. The residual head and energy dissipation rates at the stepped chute downstream end were calculated based upon the air–water flow properties. The results showed that the residual energy was the lowest for the flat stepped weir. The data for the stepped spillway configuration with in-line and staggered configurations of flat and pooled steps showed large differences in terms of residual head in the transverse direction.

Altogether the present study demonstrated that, on a 26.6° slope stepped chute, the designs with in-line and staggered configurations of flat and pooled steps did not provide any advantageous performances in terms of energy dissipation and flow aeration, but they were affected by three-dimensional patterns leading to some flow concentration. Another outcome is that some detailed physical investigations for complex stepped spillway designs are strongly recommended before any implementation into a prototype environment.

Practically, a range of design applications may include wider chutes. The staggered and in-line configurations of flat and pooled steps would consist of alternative weirs and flat steps, somehow similar to a USBR stilling basin type IX setup, but for the presence of steps. For such wide chutes, the effects of chute sidewalls would be negligible, while the effects of shock waves (at pool weir edges) would be predominant. Further experiments in wider flumes might be required to ascertain the performances of these stepped configurations in wide channels.

Acknowledgements The authors thank Jason Van Der Gevel and Stewart Matthews (The University of Queensland) for their technical assistance. They thank Professor Daniel Bung (FH Aachen University of Applied Sciences, Germany) and Dr Michael Pfister (EPFL ENAC IIC LCH, Switzerland) for their helpful comments. Some helpful discussion with Dr Masayuki Takahashi (Nihon University, Japan), is acknowledged. The useful comments of all the reviewers are acknowledged. The second writer acknowledges the financial support through a University of Queensland research scholarship. The financial support of the Australian Research Council is acknowledged (Grants ARC DP0878922 & DP120100481).

References

- André S (2004) High velocity aerated flows on stepped chutes with macro-roughness elements. Ph.D. thesis, Laboratoire de Constructions Hydrauliques (LCH), EPFL, Lausanne, Switzerland
- ASCE (1994) Alternatives for Overtopping Protection of Dams. ASCE, New York, USA, Task Committee on Overtopping Protection
- Chamani MR (2000) Air Inception in Skimming Flow Regime over Stepped Spillways. In: Proc. Intl Workshop on Hydraulics of Stepped Spillways. Balkema Publishers, Zürich, pp 61–67
- Chanson H (1994) Comparison of energy dissipation between nappe and skimming flow regimes on stepped chutes. *J Hydraul Res IAHR* 32(2):213–218 Errata: Vol. 33, No. 1, p. 113
- Chanson H (1995) Hydraulic design of stepped cascades, channels, weirs and spillways. Pergamon, Oxford
- Chanson H (2001) The hydraulics of stepped chutes and spillways. Balkema Publishers, Lisse
- Chanson H (2002) Air–water flow measurements with intrusive phase-detection probes. Can we improve their interpretation? *J Hydraul Eng ASCE* 128(3):252–255
- Chanson H (2004) Environmental hydraulics of open channel flows. Elsevier Butterworth-Heinemann, London ISBN 978 0 7506 6165 2
- Chanson H (2006) Discharge through a permeable rubble mound weir. *J Hydraul Eng ASCE* 132(4):432–433. doi:[10.1061/\(ASCE\)0733-9429](https://doi.org/10.1061/(ASCE)0733-9429)
- Chanson H (2009a) Embankment overtopping protections system and earth dam spillways, Chap. 4. In: Hayes WP, Barnes MC (eds) Dams: impact, stability and design, vol 4. Nova Science Publishers, Hauppauge, pp 101–132
- Chanson H (2009b) Turbulent air–water flows in hydraulic structures: dynamic similarity and scale effects. *Environ Fluid Mech* 9(2):125–142. doi:[10.1007/s10652-008-9078-3](https://doi.org/10.1007/s10652-008-9078-3)
- Chanson H, Carosi G (2007) Turbulent time and length scale measurements in high velocity open channel flows. *Exp Fluids* 42(3):385–401
- Chanson H, Gonzalez CA (2005) Physical modelling and scale effects of air–water flows on stepped spillways. *J Zhejiang Univ Sci* 6A(3):243–250
- Chanson H., Toombes L. (2001) Experimental Investigations of Air Entrainment in Transition and Skimming Flows down a Stepped Chute: Application to Embankment Overflow Stepped Spillways. Research Report CE 158, Department of Civil Engineering, University of Queensland
- Chanson H, Toombes L (2002) Air–water flows down stepped chutes: turbulence and flow structure observations. *Int J Multiph Flow* 27(11):1737–1761
- Chanson H, Yasuda Y, Ohtsu I (2002) Flow resistance in skimming flows and its modelling. *Can J Civ Eng* 29(6):809–819
- Djenidi L, Elavarasan R, Antonia RA (1999) The turbulent boundary layer over transverse square cavities. *J Fluid Mech* 395:271–294
- Felder S, Chanson H (2009a) Energy dissipation, flow resistance and gas–liquid interfacial area in skimming flows on moderate-slope stepped spillways. *Environ Fluid Mech* 9(4):427–441. doi:[10.1007/s10652-009-9130-y](https://doi.org/10.1007/s10652-009-9130-y)
- Felder S, Chanson H (2009b) Turbulence, dynamic similarity and scale effects in high-velocity free-surface flows above a stepped chute. *Exp Fluids* 47(1):1–18. doi:[10.1007/s00348-009-0628-3](https://doi.org/10.1007/s00348-009-0628-3)
- Felder S, Chanson H (2012a) Free-surface Profiles, Velocity and Pressure Distributions on a Broad-Crested Weir: a Physical study. *J Irrigation Drainage Eng ASCE* 138(12):1068–1074. doi:[10.1061/\(ASCE\)IR.1943-4774.0000515](https://doi.org/10.1061/(ASCE)IR.1943-4774.0000515)
- Felder S., Chanson H. (2012b) Air-Water Flow Measurements in Instationary Free-Surface Flows: a Triple Decomposition Technique. Hydraulic Model Report No. CH85/12, School of Civil Engineering, The University of Queensland, Brisbane, Australia
- Felder S., Fromm C., Chanson H. (2012a) Air Entrainment and Energy Dissipation on a 8.9° Slope Stepped Spillway with Flat and Pooled Steps. Hydraulic Model Report No. CH86/12, School of Civil Engineering, The University of Queensland, Brisbane, Australia, (ISBN 9781742720531)
- Felder S., Guenther P., Chanson H. (2012b) Air-Water Flow Properties and Energy Dissipation on Stepped Spillways: a Physical Study of Several Pooled Stepped Configurations. Hydraulic Model Report No. CH87/12, School of Civil Engineering, The University of Queensland, Brisbane, Australia
- Gonzalez CA, Chanson H (2008) Turbulence and cavity recirculation in air–water skimming flows on a stepped spillway. *J Hydraul Res IAHR* 46(1):65–72
- Kökpınar MA (2004) Flow over a stepped chute with and without macro-roughness elements. *Can J Civ Eng* 31(5):880–891
- Lawson JD (1987) Protection of rockfill dams and cofferdams against overflow and throughflow: The Australian experience. *Civ Eng Trans I.E.Aust* CE29(3):138–147

27. Ohtsu I, Yasuda Y, Takahashi M (2004) Flow characteristics of skimming flows in stepped channels. *J Hydraul Eng ASCE* 130(9):860–869
28. Peruginelli A, Pagliara S (2000) Energy Dissipation Comparison among Stepped Channel, Drop and Ramp Structures. In: *Proc. Intl Workshop on Hydraulics of Stepped Spillways*. Balkema Publishers, Zürich, pp 111–118
29. Peyras L, Royet P, Degoutte G (1992) Flow and energy dissipation over stepped gabion weirs. *J Hydraul Eng ASCE* 118(5):707–717
30. Pfister M, Chanson H (2012) Scale effects in physical hydraulic engineering models. *J Hydraul Res IAHR* 50(2):244–246
31. Rajaratnam N (1990) Skimming flow in stepped spillways. *J Hydraul Eng ASCE* 116(4):587–591
32. Takahashi M, Yasuda Y, Ohtsu I (2008) Flow patterns and energy dissipation over various stepped chutes. *J Irrigation Drainage Eng ASCE* 134(1):114–116 Discussion
33. Thorwarth J. (2008) *Hydraulisches Verhalten der Treppengerinne mit eingetieften Stufen - Selbstinduzierte Abflussinstabilitäten und Energiedissipation.* (Hydraulics of Pooled Stepped Spillways - Self-induced Unsteady Flow and Energy Dissipation.) Ph.D. thesis, University of Aachen, Germany (in German)
34. Toombes L. (2002) *Experimental Study of Air-Water Flow Properties on Low-Gradient Stepped Cascades.* Ph.D. thesis, Dept. of Civil Engineering, University of Queensland, Australia
35. Toombes L, Chanson H (2007) Surface waves and roughness in self-aerated supercritical flow. *Environ Fluid Mech* 7(3):259–270. doi:[10.1007/s10652-007-9022-y](https://doi.org/10.1007/s10652-007-9022-y)
36. Wood IR (1991) Air Entrainment in Free-Surface Flows. In: *IAHR Hydraulic Structures Design Manual No. 4, Hydraulic Design Considerations*. Balkema Publishers, The Netherlands